Deep-Subwavelength-Scale Directional Sensing Based on Highly Localized Dipolar Mie Resonances

Xuefeng Zhu,[1] Bin Liang,[2,*] Weiwei Kan,[2] Yugui Peng,[1] and Jianchun Cheng[2,†]
[1]School of Physics, Huazhong University of Science and Technology, Wuhan 430074, China
[2]Department of Physics, Key Laboratory of Modern Acoustics, MOE,
Collaborative Innovation Center of Advanced Microstructures,
Nanjing University, Nanjing 210093, China
(Received 24 September 2015; revised manuscript received 26 April 2016; published 23 May 2016)

This paper reports the formation of highly localized Mie resonances on a closed metasurface encapsulating a rigid core and the realization of directional sensing at deep-subwavelength scale (diameter $\sim\lambda/8$) with the proposed physical model. Based on modal-expansion and mode-matching methods, it is theoretically shown that the extremely anisotropic metasurface shell can support varied orders of Mie resonances around the rigid core. We further experimentally demonstrate that the Mie resonance with a dipolelike profile is strongly excited under the illumination of a plane wave at low frequencies, enabling the sensitive directional sensing due to the intensified and azimuthally dependent pressure field.

DOI: 10.1103/PhysRevApplied.5.054015

I. INTRODUCTION

Deep-subwavelength-scale directional sensing is highly desirable in various scenarios ranging from target localization and sonar applications to underwater communications, with the benefits that the sensing device can be kept from disturbing the measured acoustic fields or being perfectly hidden from sonar detections [1,2]. However, the wave diffraction, as one of the fundamental physical limitations, has imposed a distinctly hard constraint on realizing the directional sensing at deep-subwavelength scale. The lack of progress in this field is mainly attributed to the ultraweak and azimuthally isotropic responses of the deep-subwavelength sensor. In the past decades, novel wave manipulation in metamaterials has been a research hot spot due to many intriguing effects that challenge physical limitations in previous senses, such as invisibility cloaking [2–5], negative refraction [6], subwavelength focusing and imaging [7–9], and topological insulation [10], etc. The developments bring about various technical innovations in acoustic functional devices at an unprecedented level. Recently, the strong wave-matter interaction in metamaterials was paid increasing attention, where researchers made observations of acoustic rainbow trapping [11,12] and novel wave manipulation [13–16]. For example, Li's group has developed a type of folded structured metamaterial and observed slow wave propagation and localization in the metamaterial [13]. Later on, researchers proposed the concept of acoustic metasurfaces, which is basically a textured surface of deep-subwavelength thickness [15,16]. In stark contrast to the optical metasurface that efficiently transforms the free-space light into propagating surface plasmon polaritons through metallic resonators with spatially tuned responses, the acoustic counterpart supports tightly confined surface waves by dramatically reducing the asymptotic surface-mode frequency via subwavelength periodic features [11,17,18]. Despite the significant advances in harnessing low-frequency sound with the help of acoustic metasurfaces, directional sensing at a deep-subwavelength scale is still an unsolved problem.

In this paper, we propose a distinctive physical model by warping an open metasurface into a closed one, where the propagating surface waves will transform into the highly localized Mie resonances. We call the closed metasurfaces encapsulating rigid cores acoustic metaparticles, which are capable of supporting geometry-induced Mie resonances and thus concentrating the sound of low frequencies into a scale much smaller than the wavelength, like antennas. The marked concentration of sound energy and the azimuthally dependent pressure field of high-ordered Mie resonances provide a key solution to deep-subwavelength-scale directional sensing. In our work, the ultrathin metasurface shell of the acoustic metaparticle is carved with azimuthal periodic elongated grooves of folded geometries. We experimentally observe highly localized Mie resonances of a dipolar profile in the metaparticle under the illumination of plane waves at low frequencies, where the wavelength of airborne sound (λ) is much larger than the diameter of the metaparticle (D), viz., $\lambda \sim 8D$. At the resonant frequency, we measure the pressure field in the zigzag groove at different incident angles and demonstrate its angular dependence. The results unequivocally show that our proposed physical model is very promising in deep-subwavelength-scale

*liangbin@nju.edu.cn
†jccheng@nju.edu.cn

directional sensing, breaking the stringent limitation of wave diffraction.

II. DESIGN

The schematic diagram of metamaterial-enhanced acoustic directional sensing is displayed in Fig. 1(a). An incident plane wave carrying the resonant frequency strongly interacts with the core-shell-structured metaparticle, exciting the dipolar Mie resonance inside the particle shell. A sensor located at the core-shell interface detects the intensified pressure field with the amplitude highly related to the incident angle. Figure 1(b) shows a photo of the fabricated metaparticle. In Fig. 1(b), the total length of the zigzag groove is L, the radius of the rigid core is R_1, and the thickness of the textured shell is $R_2 - R_1$ (particle diameter $D = 2R_2$). N azimuthal periodic grooves in the shell are highly folded with the opening width being $R_2\theta_1$. In the narrow groove with rigid walls, acoustic waves propagate below the cutoff frequency, while the path is a zigzag line instead of a straight one. Previous works show that a zigzag groove in air (refractive index n_0 and mass density ρ_0) is approximately equivalent to a short one filled with the metafluid of a very large refractive index, which can be utilized to build up nonresonant metamaterials with broadband novel performances [13–15]. Here, we interpret the equivalence from another perspective of transformation acoustics. By transforming the space along the zigzag groove with the compression ratio $\beta = L/(R_2 - R_1)$ into a straight one [19], we can obtain the effective refractive index and mass density of the metafluid, viz., $n_0\beta$ and $\rho_0\beta$ in the direction along the transformed straight groove (see Appendix A). Since the refractive index of air $n_0 = 1$, the effective refractive index of metafluid takes a reduced form of $n_{\text{eff}} = L/(R_2 - R_1)$.

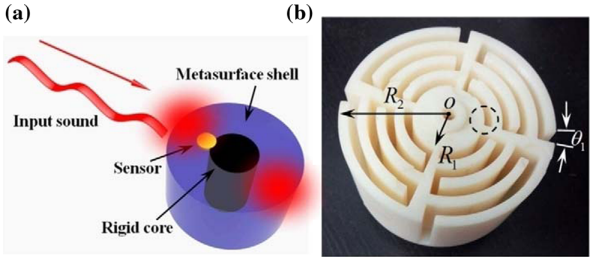

FIG. 1. (a) Schematic diagram of metamaterial-enhanced acoustic directional sensing. (b) The fabricated sample of the core-shell-structured acoustic metaparticle. In (b), the inner and outer radii of the metasurface shell are $R_1 = 1$ cm and $R_2 = 3$ cm, the total length of the zigzag groove $L \approx 12$ cm, the groove opening angle $\theta_1 = 6°$, the groove width is around 1.5 mm, and the number of folded grooves in the shell $N = 4$. The sample is fabricated by 3D printing with acrylonitrile butadiene styrene plastic. The dashed circle marks the sensor position.

III. THEORY

We employ the modal-expansion and mode-matching methods to investigate the resonance condition in our proposed physical model [20–22]. For the core-shell-structured metaparticle shown in Fig. 1(b), the pressure fields P^{I} in the shell with N grooves (region I: $R_1 \le r \le R_2$, $2m\pi/N \le \theta \le 2m\pi/N + \theta_1$, $N = 4$, $m = 0, 1, \ldots, N-1$) and P^{II} outside the metaparticle (region II: $r \ge R_2$, $0 \le \theta \le 2\pi$) are, respectively, expanded in series

$$P^{\text{I}} = \sum_{q=-\infty}^{\infty} A_q^{\text{I}} \cos[k_0 n_{\text{eff}}(r - R_1)] e^{iq\theta}, \quad (r,\theta) \in \text{region I},$$
$$P^{\text{II}} = \sum_{q=-\infty}^{\infty} A_q^{\text{II}} H_q^{(1)}(k_0 r) e^{iq\theta}, \quad (r,\theta) \in \text{region II}, \qquad (1)$$

where A_q^{I} and A_q^{II} are coefficients, $H_q^{(1)}$ is the Hankel function of the first kind, q is the mode order, k_0 is the wave number in air, and (r,θ) are the polar coordinates. Here $q = 0$, $q = 1$, and $q = 2$ correspond to Mie resonances with monopolar, dipolar, and quadrupolar profiles, respectively. From Eq. (1), we obtain that the high-ordered Mie resonances will have a very large quality factor due to the rapidly decreasing pressure field P^{II} outside the metaparticle, and the high-ordered modes can be regarded as whispering gallery modes encircling around a rigid core. When the radius of the metaparticle is much smaller than the wavelength ($R_2 \ll \lambda$), the textured shell can be regarded as an ultrathin metamaterial layer (or metasurface) with an extremely anisotropic mass density. The radial component ρ_{eff} of the density tensor is [8]

$$\rho_{\text{eff}} = 2\pi\left(\frac{2\pi - N\theta_1}{\rho_s} + \frac{N\theta_1}{n_{\text{eff}}\rho_0}\right)^{-1} \xrightarrow{\rho_s \gg \rho_0} \frac{2\pi}{N\theta_1} n_{\text{eff}}\rho_0, \qquad (2)$$

where ρ_s is the mass density of solids. By matching boundary conditions that the pressures at groove openings ($r = R_2$) are balanced and the volume velocities at the openings with suddenly changed cross sections are continued for each expanded mode (see Appendix A), we obtain

$$A_{q'}^{\text{I}} \cos[n_{\text{eff}} k_0 (R_2 - R_1)] = A_{q'}^{\text{II}} H_{q'}(k_0 R_2) - \frac{n_{\text{eff}} k_0}{\rho_{\text{eff}}} B_{q'}^{\text{I}} \sin[n_{\text{eff}} k_0 (R_2 - R_1)] = \frac{k_0}{\rho_0} A_{q'}^{\text{II}} H'_{q'}(k_0 R_2), \qquad (3)$$

where $B_{q'}^{\text{I}} = \frac{1}{2\pi}\sum_{m=0}^{N-1}\sum_q \int_{2m\pi/N}^{2m\pi/N+\theta_1} A_q^{\text{I}} e^{i(q-q')\theta} d\theta$. From Eq. (3), we further derive the following transcendental equation:

$$\frac{H_q(k_0 R_2)}{H'_q(k_0 R_2)} = -\frac{2\pi A_q^{\text{I}}}{N\theta_1 B_q^{\text{I}}} \cot[k_0 n_{\text{eff}}(R_2 - R_1)]. \qquad (4)$$

In the long-wavelength limit $k_0 R_2 \to 0$, the left term in Eq. (4) approaches zero for each mode order q, which leads to the resonance condition

$$\omega_n = (2n+1)\omega_0, \tag{5}$$

where the fundamental frequency $\omega_0 = c_0\pi/(2L)$, c_0 is the speed of sound in air, and n is the order of overtones. Equations (4) and (5) reveal that Mie resonances of different mode orders ($q \le N/2$) share very close fundamental frequencies.

The acoustic response of a metaparticle can be described by the scattering intensity that measures the total sound energy scattered from the metaparticle [23,24]. In the numerical calculations, we consider thermal damping and thboundary-layer effect in zigzag grooves and normalize the total scattered sound energy with respect to its maximum value. The mass density and speed of sound of air in free space are $\rho_0 = 1.2\ \mathrm{kg/m^3}$ and $c_0 = 343.1\ \mathrm{m/s}$, respectively. In Fig. 2, we show the normalized scattering intensity of the metaparticle as a function of frequency from 400 to 1000 Hz. The spectrum in Fig. 2 has a peak at 695 Hz (the normalized scattering intensity ~1) and a dip at 717 Hz (the normalized scattering intensity ~0.014), which takes a Fano-type profile and agrees fairly well with the eigenfrequencies of dipolar and monopolar Mie resonances with eigenfields displayed in the insets, respectively. The analytic description of dipolar and monopolar Mie resonances is studied in detail in Appendix A via modal-expansion and mode-matching methods. Because of the symmetry of eigenmode and time reversal, we will obtain that the monopolar resonance can be best excited by cylindrical-type incident waves. Eigenfrequencies of the fundamental Mie resonances can also be predicted by

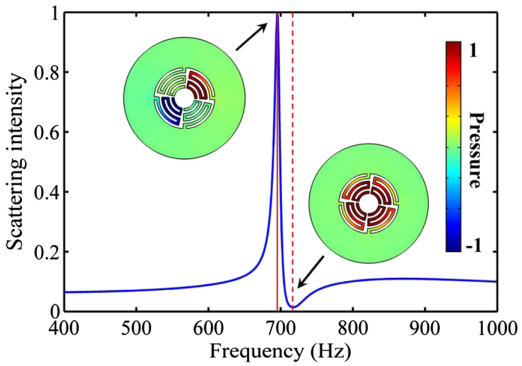

FIG. 2. The scattering intensity (arb. units) of the core-shell-structured acoustic metaparticle under the illumination of plane waves. The carrying frequencies of airborne sound are from 400 to 1000 Hz. The insets show the eigenfields of Mie resonances of monopolar and dipolar profiles, where the eigenfrequencies are marked by the dashed line and the solid line, respectively. In the calculations, we consider the thermal damping and boundary-layer effect in the zigzag grooves. The pressure is normalized with an arbitrary unit.

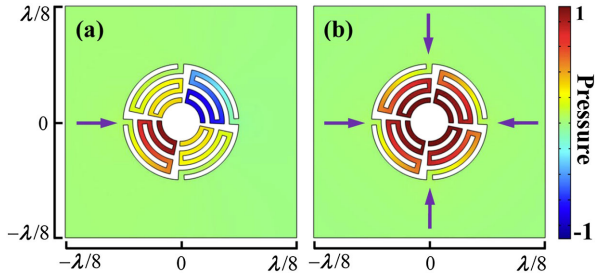

FIG. 3. (a) The excitation of a dipolar Mie resonance under the illumination of a plane wave from the left side. (b) The excitation of a monopolar Mie resonance under the illumination of four in-phase plane waves propagating towards the metaparticle from the left side, the right side, the up side, and the down side, respectively. The carrying frequency of incident plane waves is 695 Hz, where the corresponding wavelength $\lambda \approx 49$ cm. The pressure is normalized with an arbitrary unit.

Eq. (5) with $N = 4$ and $L \approx 12$ cm, which share very close values for different orders ($q \le 2$) at around 715 Hz. The result in Fig. 3(a) clearly shows that the dipolar Mie resonance ($q = 1$) is strongly excited in the metaparticle under the illumination of a plane wave at 695 Hz, while the monopolar Mie resonance ($q = 0$) is largely suppressed for the mismatched eigenfield symmetry. If we want to excite the monopolar Mie resonance, we need to employ cylindrical incoming waves or at least four in-phase plane waves propagating towards the metaparticle from the left side, the right side, the up side, and the down side, respectively, as shown in Fig. 3(b), which is virtually impossible in reality. The physics of Mie resonances can also be interpreted by a direct analog with harmonic oscillators, e.g., a vibrating string having two fixed ends. In our case, we assume that the walls of zigzag grooves are rigid. Therefore, the pressure amplitude is at a maximum at the groove bottom with the normal particle velocity that is proportional to the gradient of the pressure field being zero. As revealed by the insets of Fig. 2, the eigenfields of Mie resonances are highly confined inside the metaparticle, so that the pressure amplitude at the groove opening rapidly decays down to zero, thus giving rise to a maximal particle velocity. The above-mentioned boundary conditions indicate that the zigzag groove with a closed bottom can support stable standing waves, where the node and the antinode of sound pressure are located at the groove opening and bottom, respectively. As a compelling analog, a vibrating string having nodes at the ends will have different overtones of vibrations, and only an odd number of ordered overtones can be excited if the antinode fixes at the center, in remarkable agreement with Eq. (5). It is worth mentioning that a quadrupolar Mie resonance ($q = 2$) has a much larger Q factor than monopolar and dipolar resonances, as is demonstrated in previous works [20–22]. As a result, the quadrupolar mode is highly suppressed by intrinsic thermal damping and the boundary-layer effect in zigzag grooves of acoustic metaparticles. We also point out that a quadrupolar

Mie resonance cannot be excited by plane waves even in lossless cases due to the eigenfield mismatch.

In the following section, we will investigate only the excited dipolar resonance at the fundamental frequency of 695 Hz, where the wavelength of airborne sound is around 8 times larger than the diameter of the metaparticle ($\lambda \approx 8D$). We envision that the dipolelike resonance in the metaparticle brings about many useful properties, for example, a remarkable concentration of sound energy at the deep-subwavelength scale and, in particular, an azimuthally dependent localized pressure field. Those impressive properties make the acoustic metaparticle perform like a receiving dipolar antenna which can be utilized for sensitive directional sensing.

IV. EXPERIMENT

In the experimental demonstration, we first perform the measurement of enhanced pressure fields inside the metaparticle, where a 1/4-inch-diameter Brüel & Kjær type-4961 microphone is integrated to form an active metamaterial sensing device. During the measurement process, we keep the orientation of the groove in which a microphone (or sensor) is located directly pointing to the 10-cm-diameter loudspeaker 4 m away from the metaparticle, shown by the inset of Fig. 4. The measurement is carried out in the anechoic chamber to reduce undesired back reflections from the environment (see Appendix B). The result in Fig. 4 clearly indicates that there is more than 10 times pressure amplification at the sensor position for a 695-Hz incident plane wave, in good agreement with the numerical prediction of thermoacoustic studies. The nontrivial pressure gain is believed to be the result of the Mie resonance of a dipolar profile as shown in Fig. 2. We also point out that there is a trade-off between the folding degree and pressure gain. An increase in the folding degree always leads to a decrease in the pressure gain, where more significant dissipation is introduced due to viscosity and thermal loss in narrow air channels. For an active metamaterial device, choosing a moderate size of $R_2 = 3$ cm and groove width of 1.5 mm can reach a good compromise between the pressure gain and resonance loss. Therefore, we still achieve a distinctive pressure gain ($10 \sim 20$ times) in the scale of around 1/8 wavelength.

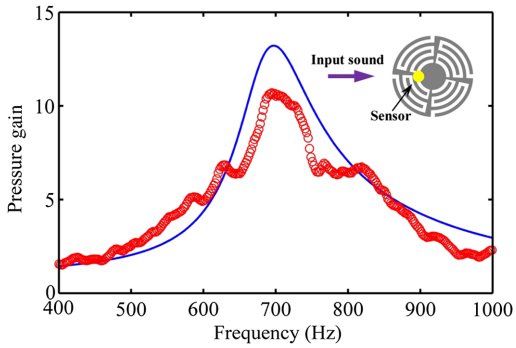

FIG. 4. The pressure-gain (arb. units) spectra measured at the sensor position inside the metaparticle. The circle dots represent the experimental data and the solid line represents the simulation result. The inset shows the direction of input sound with respect to the orientation of the groove in which the sensor is located.

Next, we demonstrate that the core-shell-structured metaparticle exhibits a remarkable directional response. Figure 5(a) plots the normalized pressure amplitudes calculated at the sensor position *versus* the angle of incidence at 695 Hz with or without a metasurface shell. In the figure, the pressure amplitude is varied with respect to the incident angle of plane waves, when the metasurface shell is utilized. Even though the acoustic response of the metaparticle is less anisotropic in consideration of viscosity and thermal damping by comparing the red thick line with the blue dashed line in Fig. 5(a), we still can locate the

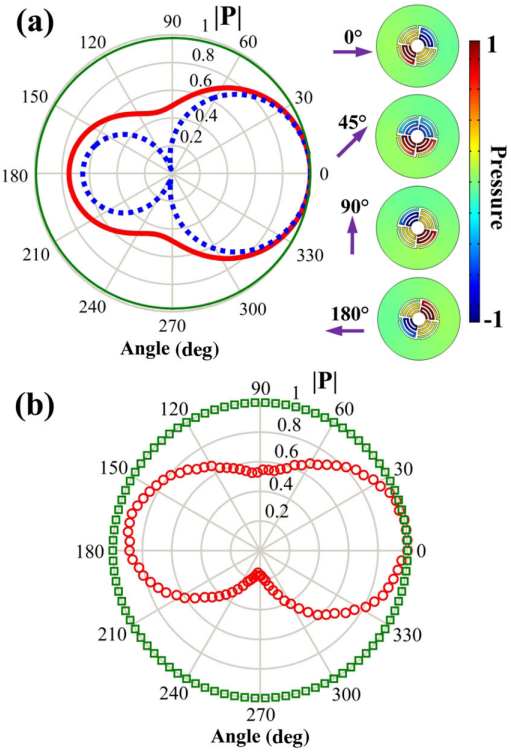

FIG. 5. (a) The normalized pressure amplitudes calculated at the sensor position [referring to the inset of Fig. 4] versus the angle of incidence with or without a metasurface shell. For the core-shell-structured metaparticle, the red thick line represents the calculation result in consideration of thermal damping and boundary-layer effect, while the blue dashed line shows the result in the lossless case. When the metasurface shell is removed, we will obtain the green thin line that indicates isotropic sensor responses. The right-hand side displays the distributions of pressure fields inside the metaparticle at four different incident angles. (b) The normalized pressure amplitudes experimentally measured at the sensor position versus the angle of incidence with (red circles) or without (green squares) utilizing the metasurface shell. The pressure is normalized with an arbitrary unit.

position of the far-field sound source after a complete rotation. We also convincingly prove the sensor response is closely isotropic from the green thin line in Fig. 5(a) after the metasurface shell is removed. Pressure field distributions for different incident angles are shown at the right-hand side of Fig. 5(a). Acoustic waves at a 0° incident angle (incident from the left) can excite dipolar Mie resonances with the field mainly localized in the zigzag grooves with openings orienting towards the left and right, and the largest acoustic response is obtained by noting that the sensor locates at the bottom of the left groove. While at a 90° incident angle, the acoustic response is at a minimum because the fields of the excited dipolar resonances are mainly confined in the zigzag grooves with openings orienting towards up and down directions, in orthogonal relation with the case of 0° incidence. The ratio of the maximum and minimum acoustic responses is about 2.3. We can deal with the 45° incidence case as the superposition of 0° and 90° incidences, where the pressure field in each of four grooves is less intensified. It is also worth noting that the acoustic metaparticle sensor can, in principle, distinguish signals emitted from opposite directions for the slightly different intensities of received signals, viz., the normalized pressure amplitude ∼1 for 0° incidence and ∼0.75 for 180° incidence. Figure 5(b) shows the measured directivity patterns of acoustic sensor responses with or without utilizing a metasurface shell. During measurement processes, we first mount the core-shell-structured metaparticle on a rotary motor with a rotation step of 4°. The measured data are fairly consistent with the simulated data by comparing the red thick line in Fig. 5(a) with the red circles in Fig. 5(b), where the normalized pressure amplitudes measured at the sensor position are ∼1 for 0° incidence, ∼0.53 for 90° incidence, ∼0.89 for 180° incidence, and ∼0.15 for 270° incidence. Then we remove the metasurface shell and measure the sensor response in a complete rotation. As shown by the green squares in Fig. 5(b), the experimental data demonstrate that the acoustic response is isotropic, while the sensor size is deep subwavelength and no Mie resonance is excited. In the end, it should be pointed out that the acoustic metaparticle is not restricted to the in-plane directional sensing. We can also employ it to locate the far-field sound source positioned out of plane. The measured acoustic response *versus* the tilted angle of the metaparticle is shown in Appendix B.

V. SUMMARY AND OUTLOOK

In summary, we clearly demonstrate the superior properties of core-shell-structured acoustic metaparticles, such as concentrating input sound energy in deep-subwavelength scale (diameter $\sim\lambda/8$) and supporting the Mie resonances with azimuthally dependent pressure field distributions. We employ the modal-expansion and mode-matching methods to deduce the resonance condition and experimentally observe the excitation of the Mie resonance with a dipolar profile under the illumination of plane waves. Utilizing the intensified and azimuthally dependent pressure field of the Mie resonance, we experimentally demonstrate sensitive directional sensing at deep-subwavelength scale. The proposed physical model may find profound impacts in vector sensing, wave-front engineering, as well as fundamental explorations of nonreciprocal acoustics in combination with nonlinearity and time varying.

ACKNOWLEDGMENTS

This work was supported by the National Basic Research Program of China (973 Program) (Grants No. 2010CB327803 and No. 2012CB921504), the National Natural Science Foundation of China (Grants No. 11404125, No. 11174138, No. 11174139, No. 11222442, No. 81127901, and No. 11274168), NCET-12-0254, and a project funded by the Priority Academic Program Development of Jiangsu Higher Education Institutions. X. F. Z. and Y. G. P. acknowledge the financial support from the Bird Nest Plan of HUST.

APPENDIX A: ANALYTICAL DERIVATIONS

1. Transformation acoustics and the folded mapping

In the long-wavelength regime, acoustic waves propagate below the cutoff frequency [13]. A zigzag path is therefore approximately equivalent to a long straight one in Fig. 6. Based on transformation acoustics, the relation of material parameters between a long groove in air (coordinates x-y, length L, bulk modulus κ_0, and mass density ρ_0) and a short one filled with metafluid (coordinates x'-y', length l, bulk modulus κ_{eff}, and mass density ρ_{eff}) can be written as $\boldsymbol{\rho}_{\text{eff}}{}^{-1} = \boldsymbol{H}\boldsymbol{\rho}_0{}^{-1}\boldsymbol{H}^T/\det(\boldsymbol{H})$ and $\kappa_{\text{eff}} = \det(\boldsymbol{H}) \times \kappa_0$, respectively, where $\boldsymbol{H}$ is the Jacobian matrix defined by the form of $\boldsymbol{H} = \text{diag}\{\partial x'/\partial x, \partial y'/\partial y\}$. Here, the folded mapping is specified by $x' = x/\beta$ and $y' = y$, with $\beta = L/l$ being the compression ratio. Then the parameters of metafluid are [19]

$$\boldsymbol{\rho}_{\text{eff}}(x', y') = \begin{pmatrix} \beta & 0 \\ 0 & \frac{1}{\beta} \end{pmatrix} \rho_0(x, y),$$
$$\kappa_{\text{eff}}(x', y') = \kappa_0(x, y)/\beta. \tag{A1}$$

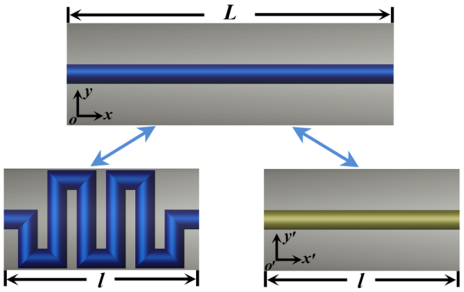

FIG. 6. Schematic of the folded mapping in transformation acoustics.

In the metafluid, the acoustic waves are apparently slowed down in the x' direction with the velocity $v_{\text{eff}} = \sqrt{\kappa_0/\rho_0}/\beta = c_0/\beta$.

In our paper, the space along the zigzag groove is transformed into a straight one with the compression ratio being $\beta = L/(R_2 - R_1)$, referring to Fig. 1. From Eq. (A1), we finally obtain the effective refractive index and mass density of the metafluid in the direction along the transformed straight groove (in the x' direction), viz.,$n_0\beta$ and $\rho_0\beta$.

2. Modal-expansion and mode-matching methods

Modal-expansion and mode-matching methods have been vastly used in optics, see Refs. [21,22]. Here, we employ the modal-expansion and mode-matching methods to determine the resonance condition of varied Mie resonances in the core-shell-structured acoustic metaparticle. As mentioned in the text, when the radius of the metaparticle is much smaller than the free-space wavelength ($R_2 \ll \lambda$), the textured shell can be regarded as an ultrathin metamaterial layer (or metasurface) with an extremely anisotropic mass density. The radial component ρ_{eff} of the density tensor is

$$\rho_{\text{eff}} = 2\pi\left(\frac{2\pi - N\theta_1}{\rho_s} + \frac{N\theta_1}{n_{\text{eff}}\rho_0}\right)^{-1} \overset{\rho_s \gg \rho_0}{\longrightarrow} \frac{2\pi}{N\theta_1} n_{\text{eff}}\rho_0, \quad \text{(A2)}$$

where ρ_s is the mass density of solids and N is the groove number. For the core-shell-structured metaparticle shown in Fig. 7, the pressure fields P^{I} in the shell with N grooves (region I: $R_1 \le r \le R_2$, $2m\pi/N \le \theta \le 2m\pi/N + \theta_1$, $N = 4$, $m = 0, 1, \ldots, N-1$) and P^{II} outside the metaparticle (region II: $r \ge R_2$, $0 \le \theta \le 2\pi$) are, respectively, expanded in series

$$P^{\text{I}} = \sum_{q=-\infty}^{\infty} A_q^{\text{I}} \cos[k_0 n_{\text{eff}}(r - R_1)] e^{iq\theta}, \quad (r,\theta) \in \text{region I},$$
$$P^{\text{II}} = \sum_{q=-\infty}^{\infty} A_q^{\text{II}} H_q^{(1)}(k_0 r) e^{iq\theta}, \quad (r,\theta) \in \text{region II}, \quad \text{(A3)}$$

where A_q^{I} and A_q^{II} are coefficients, $H_q^{(1)}$ is the Hankel function of first kind, q is the mode order, k_0 is the wave number in air, and (r, θ) are the polar coordinates. $q = 0$, $q = 1$, and $q = 2$ correspond to Mie resonances with monopolar, dipolar, and quadrupolar profiles, respectively.

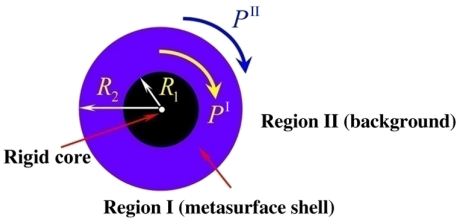

FIG. 7. Schematic of the modal-expansion and mode-matching methods in analyzing the resonance condition of the core-shell-structured acoustic metaparticle.

The resonance condition for Mie resonances is obtained by matching boundary conditions, where the pressures at groove openings are balanced

$$P^{\text{I}}\Big|_{r=R_2, 2m\pi/N \le \theta \le 2m\pi/N+\theta_1} = P^{\text{II}}\Big|_{r=R_2, 2m\pi/N \le \theta \le 2m\pi/N+\theta_1}, \quad \text{(A4)}$$

and the volume velocities at the openings with suddenly changed cross sections are continued for each expanded mode

$$-\frac{1}{i\omega\rho_{\text{eff}}} \sum_{m=0}^{N-1} \int_{2m\pi/N}^{2m\pi/N+\theta_1} \frac{\partial P^{\text{I}}}{\partial r} e^{-iq'\theta} d\theta \Big|_{r=R_2} = -\frac{1}{i\omega\rho_0} \int_0^{2\pi} \frac{\partial P^{\text{II}}}{\partial r} e^{-iq'\theta} d\theta \Big|_{r=R_2}. \quad \text{(A5)}$$

By substituting Eq. (A3) into Eqs. (A4) and (A5), we obtain

$$A_{q'}^{\text{I}} \cos[n_{\text{eff}} k_0 (R_2 - R_1)] = A_{q'}^{\text{II}} H_{q'}(k_0 R_2) - \frac{n_{\text{eff}} k_0}{\rho_{\text{eff}}} B_{q'}^{\text{I}} \sin[n_{\text{eff}} k_0 (R_2 - R_1)] = \frac{k_0}{\rho_0} A_{q'}^{\text{II}} H'_{q'}(k_0 R_2), \quad \text{(A6)}$$

where $B_{q'}^{\text{I}} = \frac{1}{2\pi} \sum_{m=0}^{N-1} \sum_q \int_{2m\pi/N}^{2m\pi/N+\theta_1} A_q^{\text{I}} e^{i(q-q')\theta} d\theta$. After some arithmetic deductions from Eq. (A6), we consequently derive the following transcendental equation:

$$\frac{H_q(k_0 R_2)}{H'_q(k_0 R_2)} = -\frac{2\pi A_q^{\text{I}}}{N\theta_1 B_q^{\text{I}}} \cot[k_0 n_{\text{eff}}(R_2 - R_1)]. \quad \text{(A7)}$$

In the long-wavelength limit, *viz.*, $x = k_0 R_2 \to 0$, the Hankel function of first kind is approximated into

$$\lim_{x\to 0} H_q(x) = \begin{cases} \frac{2i}{\pi} \ln(\frac{x}{2}), & q = 0, \\ -\frac{\Gamma(q)}{\pi} (\frac{2}{x})^q, & q > 0, \end{cases} \quad \text{(A8)}$$

for different orders, where $\Gamma(\cdot)$ is the Gamma function. Therefore, the left term in Eq. (A7) is approaching zero since

$$\lim_{x\to 0} \frac{H_q(x)}{H'_q(x)} = \begin{cases} \lim_{x\to 0} x \ln(\frac{x}{2}) \to 0, & q = 0, \\ \lim_{x\to 0} \frac{-x}{q} \to 0, & q > 0. \end{cases} \quad \text{(A9)}$$

From Eqs. (A7) and (A9), it is apparent that Mie resonances of different mode orders ($q \le N/2$) share very close

resonant frequencies and the resonant frequencies correspond to zero points of the right term of Eq. (A7), which directly leads to

$$\omega_n = (2n+1)\omega_0, \tag{A10}$$

where the fundamental frequency $\omega_0 = c_0\pi/(2L)$, c_0 is the speed of sound in air, and n is the order of overtones. Principally, the modal-expansion and mode-matching methods can be also extended into the study of Mie resonances in spherical metaparticles by means of spherical harmonic expansion and mode matching, due to the fact that acoustic waves can propagate within the folded channels of deep-subwavelength cross sections in the absence of a cutoff frequency.

APPENDIX B: THE EXPERIMENTAL MEASUREMENTS

1. Measurement tips

In the experiment (Fig. 8), we perform the measurement of enhanced pressure fields inside the metaparticle through a 1/4-inch-diameter Brüel & Kjær type-4961 microphone integrated on the top. The data are recorded with a Brüel & Kjær PULSE 3160-A-042 multichannel analyzer. The frequency response is obtained with SSR analysis of Brüel & Kjær PULSE software LABSHOP version 13.5.10.

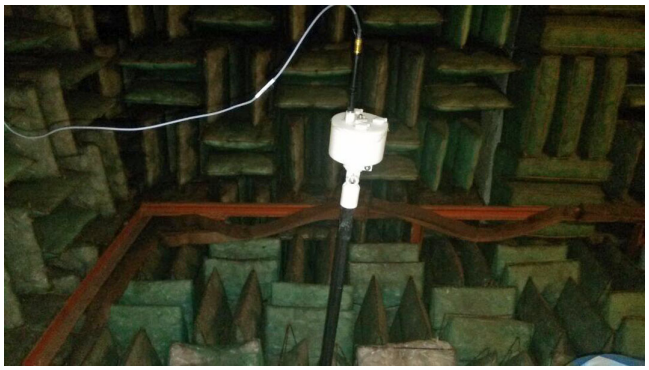

FIG. 8. Photo of the active metamaterial sensing device.

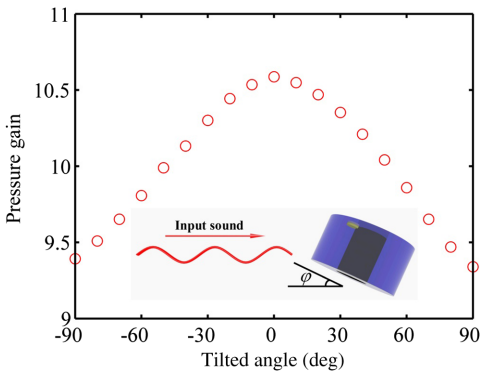

FIG. 9. The pressure gain (arb. units) experimentally measured at the sensor position *versus* the tilted angle of the metaparticle.

During the measurement of directional responses, the metaparticle is mounted on a rotary motor with a rotation step of 4°. We keep the 10-cm-diameter loudspeaker 4 m away from the metaparticle. The measurement is carried out in the anechoic chamber to reduce undesired back reflections from the environment.

2. Measured acoustic response to the sound source positioned out of plane

From the measurement result (Fig. 9), the acoustic response reaches a maximum when the sound source is located in plane (or $\varphi = 0°$). Therefore, to target a sound source in 3D space, we first tilt the metaparticle to get the φ at the maximum response, and then rotate the metaparticle to finally determine the position of the sound source based on the rule shown in Fig. 5.

[1] A. Alù and N. Engheta, Cloaking a Sensor, Phys. Rev. Lett. **102**, 233901 (2009).

[2] X. Zhu, B. Liang, W. Kan, X. Zou, and J. Cheng, Acoustic Cloaking by a Superlens with Single-Negative Materials, Phys. Rev. Lett. **106**, 014301 (2011).

[3] S. Zhang, C. Xia, and N. Fang, Broadband Acoustic Cloak for Ultrasound Waves, Phys. Rev. Lett. **106**, 024301 (2011).

[4] B. I. Popa, L. Zigoneanu, and S. A. Cummer, Experimental Acoustic Ground Cloak in Air, Phys. Rev. Lett. **106**, 253901 (2011).

[5] X. Zhu, H. Ramezani, C. Shi, J. Zhu, and X. Zhang, *PT*-Symmetric Acoustics, Phys. Rev. X **4**, 031042 (2014).

[6] K. Li, Y. G. Peng, X. F. Zhu, J. T. Zhang, H. J. Lv, and S. C. Liu, Observation of unidirectional negative refraction in an acoustic metafluid prism, Appl. Phys. Lett. **104**, 043505 (2014).

[7] S. Zhang, L. Yin, and N. Fang, Focusing Ultrasound with an Acoustic Metamaterial Network, Phys. Rev. Lett. **102**, 194301 (2009).

[8] J. Li, L. Fok, X. Yin, G. Bartal, and X. Zhang, Experimental demonstration of an acoustic magnifying hyperlens, Nat. Mater. **8**, 931 (2009).

[9] J. Zhu, J. Christensen, J. Jung, L. Martin-Moreno, X. Yin, L. Fok, X. Zhang, and F. J. Garcia-Vidal, A holey-structured metamaterial for acoustic deep-subwavelength imaging, Nat. Phys. **7**, 52 (2011).

[10] X. F. Zhu, Y. G. Peng, X. Y. Yu, H. J M. Bao, Y. X. Shen, and D. G. Zhao, Topologically protected acoustic helical edge states and interface states in strongly coupled metamaterial ring lattices, arXiv:1508.06243.

[11] J. Zhu, Y. Chen, X. Zhu, F. J. Garcia-vidal, X. Yin, W. Zhang, and X. Zhang, Acoustic rainbow trapping, Sci. Rep. **3**, 1728 (2013).

[12] Y. Chen, H. Liu, M. Reilly, H. Bae, and M. Yu, Enhanced acoustic sensing through wave compression and pressure

amplification in anisotropic metamaterials, Nat. Commun. **5**, 5247 (2014).
[13] Z. Liang and J. Li, Extreme Acoustic Metamaterial by Coiling Up Space, Phys. Rev. Lett. **108**, 114301 (2012).
[14] Y. Xie, B.-I. Popa, L. Zigoneanu, and S. A. Cummer, Measurement of a Broadband Negative Index with Space-Coiling Acoustic Metamaterials, Phys. Rev. Lett. **110**, 175501 (2013).
[15] Y. Xie, A. Konneker, B.-I. Popa, and S. A. Cummer, Tapered labyrinthine acoustic metamaterials for broadband impedance matching, Appl. Phys. Lett. **103**, 201906 (2013).
[16] Y. Li, B. Liang, T. Xu, X. Zhu, X. Zou, and J. Cheng, Acoustic focusing by coiling up space, Appl. Phys. Lett. **101**, 233508 (2012).
[17] N. Yu, P. Genevet, M. A. Kats, F. Aieta, J. Tetienne, F. Capasso, and Z. Gaburro, Light propagation with phase discontinuities: Generalized laws of reflection and refraction, Science **334**, 333 (2011).
[18] S. Sun, Q. He, S. Xiao, Q. Xu, X. Li, and L. Zhou, Gradient-index meta-surfaces as a bridge linking propagating waves and surface waves, Nat. Mater. **11**, 426 (2012).
[19] W. Kan, B. Liang, X. Zhu, R. Li, X. Zou, H. Wu, J. Yang, and J. Cheng, Acoustic illusion near boundaries of arbitrary curved geometry, Sci. Rep. **3**, 1427 (2013).
[20] A. Pors, E. Moreno, L. Martin-Moreno, J. B. Pendry, and F. J. Garcia-Vidal, Localized Spoof Plasmons Arise While Texturing Closed Surfaces, Phys. Rev. Lett. **108**, 223905 (2012).
[21] R. Garcia-Salgado, V. M. Garcia-Chocano, D. Torrent, and J. Sanchez-Dehesa, Negative mass density and ρ-near-zero quasi-two-dimensional metamaterials: Design and applications, Phys. Rev. B **88**, 224305 (2013).
[22] P. A. Huidobro, X. Shen, J. Cuerda, E. Moreno, L. Martin-Moreno, F. J. Garcia-Vidal, T. J. Cui, and J. B. Pendry, Magnetic Localized Surface Plasmons, Phys. Rev. X **4**, 021003 (2014).
[23] N. Kundtz, D. Gaultney, and D. R. Smith, Scattering cross-section of a transformation optics-based metamaterial cloak, New J. Phys. **12**, 043039 (2010).
[24] Y. Cheng, C. Zhou, B. G. Yuan, D. J. Wu, Q. Wei, and X. J. Liu, Ultra-sparse metasurface for high reflection of low-frequency sound based on artifical Mie resonances, Nat. Mater. **14**, 1013 (2015).